



Spatial Relations of Earthquake Induced Landslides Triggered by 2015 Gorkha Earthquake $M_w = 7.8$

Kaushal R. Gnyawali and Basanta R. Adhikari

Abstract

This paper presents the results of an extensive mapping of co-seismic landslides triggered by the 2015 Gorkha earthquake in central Nepal. More than 19,332 landslides have been identified covering 61.5 km² of land in about 20,500 km² area of investigation using Google Earth imagery. Their spatial distribution characteristics and relation to the triggering mechanism is studied. Interesting regional localization and angular distribution characteristics, more controlled by the rupture directivity is observed. Seismic, geomorphic and lithological parameters that induce susceptibility to their occurrence is studied using two indices of landslide concentration: Landslide Area Percentage (LAP) and Landslide Number Percentage (LNP) in comparison with % area of each parameter classes. Positive correlation with the chosen triggering parameters are observed but there are some significant differences in the parameter values and distribution plots to co-seismic landslides in other parts of world. These results provide valuable information about the slope response characteristics in case of seismic activation in thrust faulting Himalayan landscapes, and this is important in further researches on co-seismic landslide prediction models for mountainous settlements, sediment yield studies and cascading landslide disasters after major earthquakes.

Keywords

Gorkha earthquake • Landslides • Spatial distribution • Nepal Himalaya

Introduction

In mountainous regions, strong earthquakes trigger thousands of landslides in a wide area and in a short interval of time. These landslides evolve a secondary chain of disasters e.g. damage to settlements, landslide dams and flooding, blockade of lifelines and roads and damage to the

infrastructure in a situation of emergency rescue and frequently occurring aftershocks (Cui et al. 2011). It is necessary to properly understand their nature of occurrence in relation to their triggering mechanism, which is a delicate interplay of the strong ground motion (e.g. fault plane geometry, rupture directivity and ground acceleration), geomorphological (e.g. absolute elevation, slope angle, slope orientation, curvature) and lithological characteristics at a site. This understanding is essential for the improvement of spatial earthquake induced landslide prediction models, which are critical to minimizing the hazard in mountainous areas with development and implementation of hazard maps and land-use policies (e.g. Xu et al. 2012; Dimri et al. 2007).

On 25 April 2015, at 11:56 a.m., Nepal Standard Time, a catastrophic earthquake $M_w = 7.8$ shook much of central Nepal, along the Main Himalayan Thrust fault and resulting

K.R. Gnyawali (✉)

Institute of Engineering, Khwopa College of Engineering,
Department of Civil Engineering, Tribhuvan University,
Libali-02, 44800 Bhaktapur, Nepal
e-mail: kaushal.raj.gnyawali@gmail.com

B.R. Adhikari

Institute of Engineering, Pulchowk Campus, Department of Civil
Engineering, Tribhuvan University, 44700 Lalitpur, Nepal
e-mail: bradhikari@ioe.edu.np

over 8856 fatalities and 22,309 injured (Government of Nepal 2016). The main shock epicentre (28.147°N, 84.708°E) was located in Gorkha district, with focal depth ~15 km, which was followed by numerous aftershocks over the next several weeks (Adhikari et al. 2015; USGS 2016). The earthquake triggered more than 19,332 landslides, avalanches, and rockslides above and near the rupture zone covering 61.5 km² area of landmass degradation and comprising the area of investigation (AOI) = 20,500 km². Scrutinizing co-seismic landslide distribution is essential for understanding the nature of earthquakes in the region and predicting susceptible landslide areas in future earthquakes. Earlier studies of the earthquake triggered landslide distribution and simple spatial correlation have been summarized by Keefer (1984, 2000, 2002) and Rodríguez (1999). The focus on the relation between the landslides and the triggering seismic factors- e.g. magnitude, distance to epicenter/fault rupture, peak ground acceleration (PGA) rupture, peak ground acceleration (PGA) and static hill slope condition, geomorphologic factors- e.g. slope, aspect, topographic position and geology is key to understanding their nature of occurrence. This has been analyzed after many large earthquakes e.g. Mw = 6.6 Chuetsu, Japan (Wang et al. 2007); Mw = 7.9 Wenchuan, China (Qi et al. 2010; Dai et al. 2011; Xu et al. 2014a); Mw = 7.0 Port-au-Prince, Haiti (Xu et al. 2014b). Previous efforts of studies on landslides triggered by the Gorkha earthquake based on field reconnaissance have been compiled (e.g. Collins and Jibson 2015; Hashash et al. 2015) and their spatial distribution characteristics with mapped 4312 coseismic landslides has been discussed in (Kargel et al. 2016). However, this study considers larger number of mapped landslides with area polygons and geomorphological comparisons (Fig. 2).

The main purpose of this study is to characterize the spatial distribution of landslides triggered by the Gorkha earthquake and correlating their occurrence with the triggering mechanisms: strong ground motion (e.g. PGA, seismogenic-fault), geomorphology (e.g. slope, aspect, curvature) and lithology, using two proxies of the co-seismic landslide abundance—(1) landslide area percentage (LAP) and (2) landslide top number percentage (LNP) to the percentage of class area in each parameter within the Area of Influence, AoI (i.e. 20,500 km²). The LAP is defined as % area of landslides out of total landslide area (i.e. 61.5 km²) in the class area within AoI. The LNP is defined as % number of landslides out of total landslide number (i.e. 19,332) in the class area within AoI. Overall landslide area density, defined as % of landslide area to total area of investigation was found to be $(61.5 / 20,500 * 100\%) = 0.3\%$ and landslide number density is $(19,332 \text{ nos.} / 20,500 \text{ km}^2) = 0.94$ landslides per square kilometer.

Tectonic Setting

The Gorkha earthquake ruptured along 120 km west-to-east of the Main Himalayan Thrust (MHT) (a shallow dipping megathrust) system (Grandin et al. 2015; Elliott et al. 2016), which is the main boundary interface between the subducting Indian plate and the overriding Eurasian plate to the north and accommodates half the India-Eurasia convergence -avg. 20 mm/year (e.g. Bilham et al. 1997; Bettinelli et al. 2006). Four major fault systems run east- west of region including main frontal thrust(MFT), main boundary thrust (MBT), main central thrust(MCT) and South Tibetan Detachment System (STDS) from south to north; the first three of which comprise the HFT system (Bollinger et al. 2006) and the fourth marks the boundary of Indian and Eurasian plate. The spatio-temporal evolution of aftershock epicenters reveals a clustering activity within the main shock rupture zone and narrow concentration in 40 km-wide band which is more seismically active towards the east (Adhikari et al. 2015) (Fig. 1).

Landslide Mapping and Analysis

This study comprises of two parts: (1) compilation of the earthquake triggered landslide inventory and (2) Overlay analysis with the geomorphological, seismic and lithological parameter- vectors and raster layers in Geographic Information System (GIS).

Earthquake Triggered Landslide Inventory

A comprehensive landslide inventory is essential for the subsequent spatial distribution analysis, but since the earthquake triggered landslides are large in number and very widely distributed, it is impossible to perform detailed field-mapping on every landslide. Remote sensing is applied to delineate the location and boundary of each landslide. In this study, high resolution true color optical satellite (RGB visible band) images available in Google Earth (GE) are used to map the landslides. A spatial distribution map of the earthquake-triggered landslides was prepared in a GIS platform (Fig. 2).

Bare earth- landslide scars are identified in updated satellite imagery after the earthquake from eye altitude of 500 m (in avg.), which corresponds to approximately 1:20,000 scale. Each earthquake triggered landslide is marked by a polygon boundary- delineating its source, transportation and deposition area integrally as one landslide. Landslide crown points are also marked during this process. Most landslides (>98%) are shallow disrupted mass

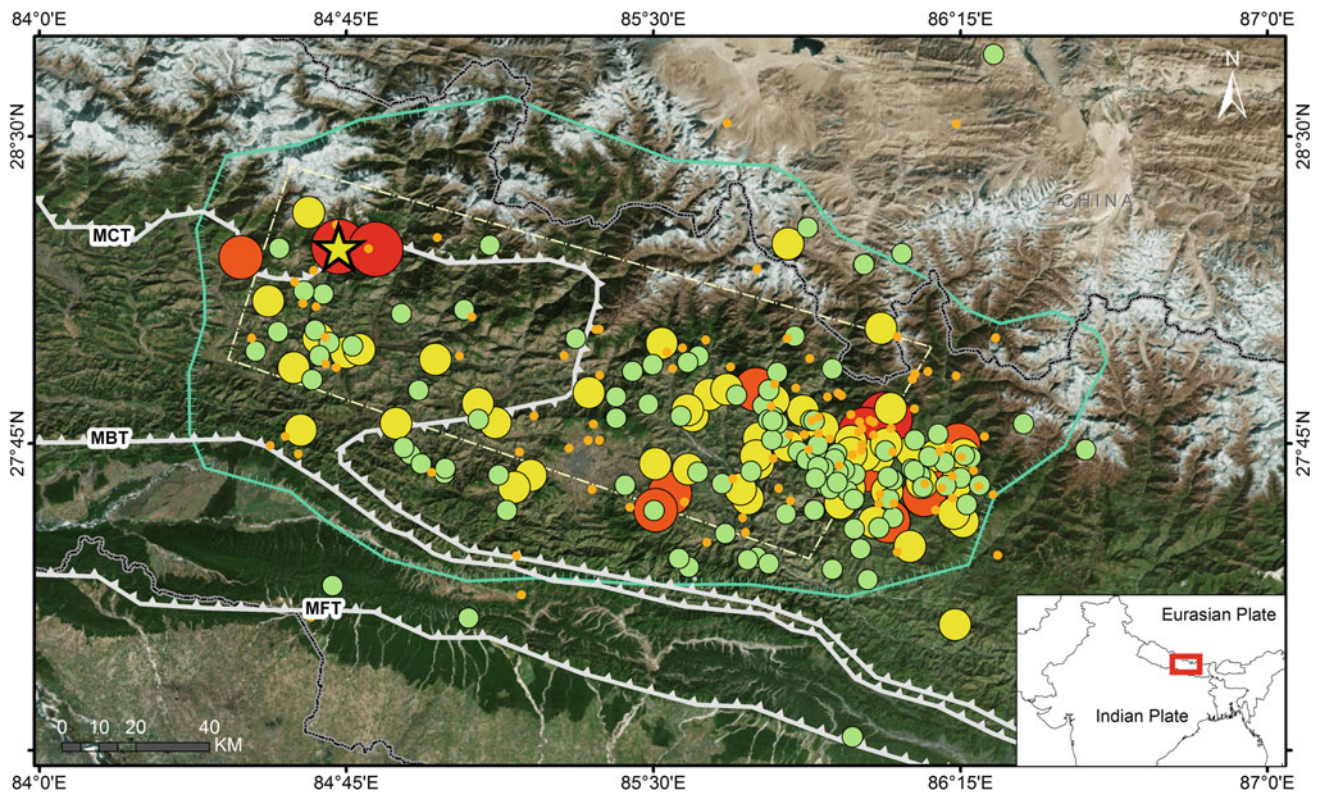


Fig. 1 Seismicity map of Gorkha Earthquake. *Yellow star* is the main shock epicenter at Gorkha the *dots* represent aftershock epicenters: (1) *Red* = 6.3–7.8 M_w , (2) *Orange* = 5.2–6.3 M_w , (3) *Yellow* = 4.6–5.2

M_w , (4) *Green* = 4.2–4.6 M_w and (5) *Golden* = < 4.2 M_w . Imagery credits ESRI basemap

where the failed mass evacuated the failure plane and moved downslope to leave evident landslide scars; rock falls and dry debris flows are also common and a very few number of large landslides also occurred (Collins and Jibson 2015; Hashash et al. 2015) (Fig. 3). Comparison of pre- and post-earthquake imagery was carried out to include only co-seismic landslides in the inventory. Since, the imagery dates vary slightly (a few days to weeks) depending upon the location, so the inventory comprises co-seismic landslides that were triggered by the main shock and succeeding aftershocks before major monsoon occurred in the region.

19,332 landslides were mapped with total area of land-mass degradation = 61.5 km². in an area of 20,500 km². The minimum area of mapped landslides with this methodology was about 20 m². Detailed criteria of distinguishing pre-earthquake, co-seismic and post-earthquake landslides listed in Xu (2014c) have been adopted as far as possible with GE imagery. In summary, all landslides recognized in the imagery and distinguished as earthquake triggered have been mapped and landslide complexes have also been divided into individual landslides.

Landslide Distribution and Density Analysis

The landslide distribution mostly seems confined within the modeled seismo-genic fault projection by (USGS 2016) and well distributed in a broad strip region where the after-shocks epicenter distribution is dense. High landslide concentration is observed in the main-shock epicenter region at Gorkha and the largest aftershock ($M_w = 7.3$) at Dolakha, which lies to south-eastern part of the main shock (towards the end of rupture). The distribution runs almost parallel to the main frontal thrust (MFT) trace of the Main Himalaya Thrust system, at a distance, which was actually the source of strain breakage during the earthquake (Elliott et al. 2016). Less number of landslides seem to occur outside this zone, indicating a strong localized zone of seismic activity. The landslide number density, computed as number of landslides per kilometers' square, increases from the main shock epicenter towards the South-East-East. Apparently, they seem to have a strong angular pattern to the main-shock epicenter, where most landslides seem to be aligned on mostly 140°–180° angular belt on the SEE direction to the main shock

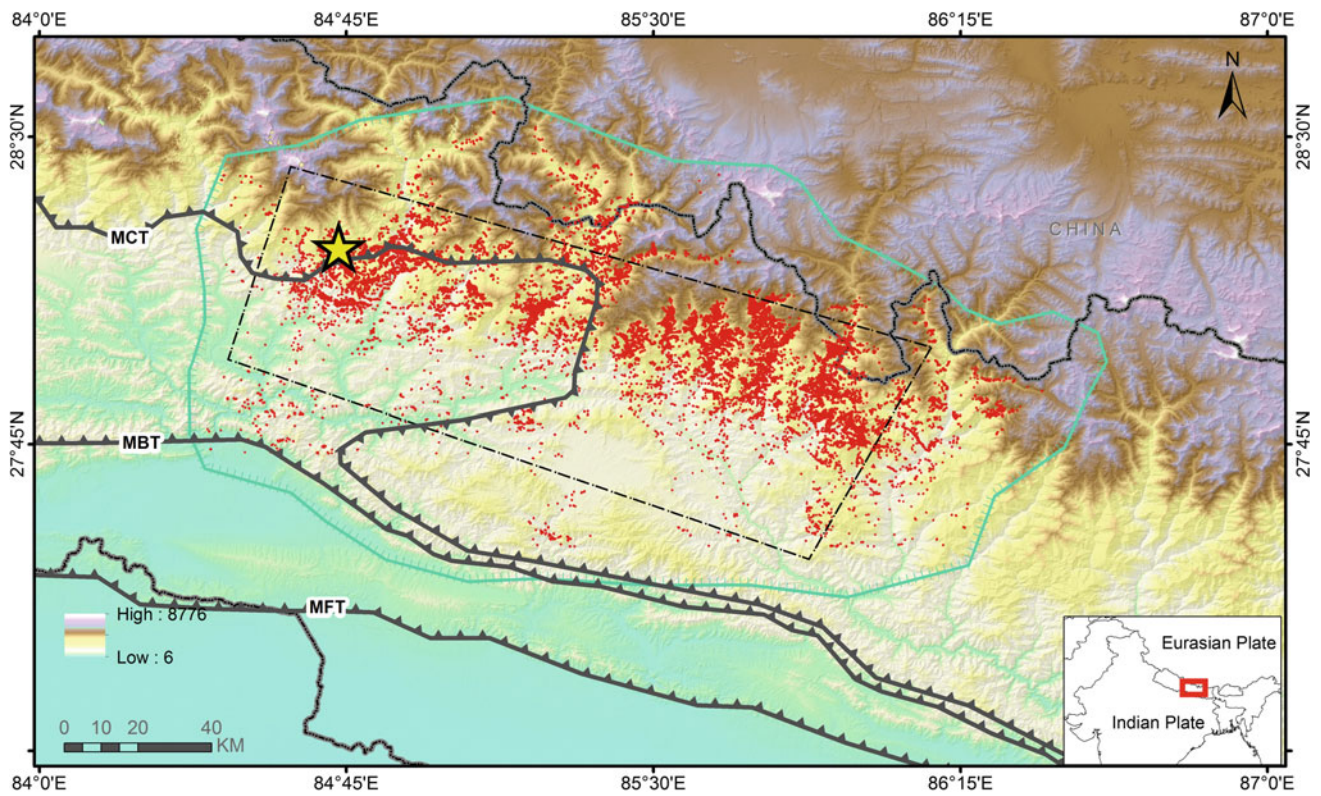
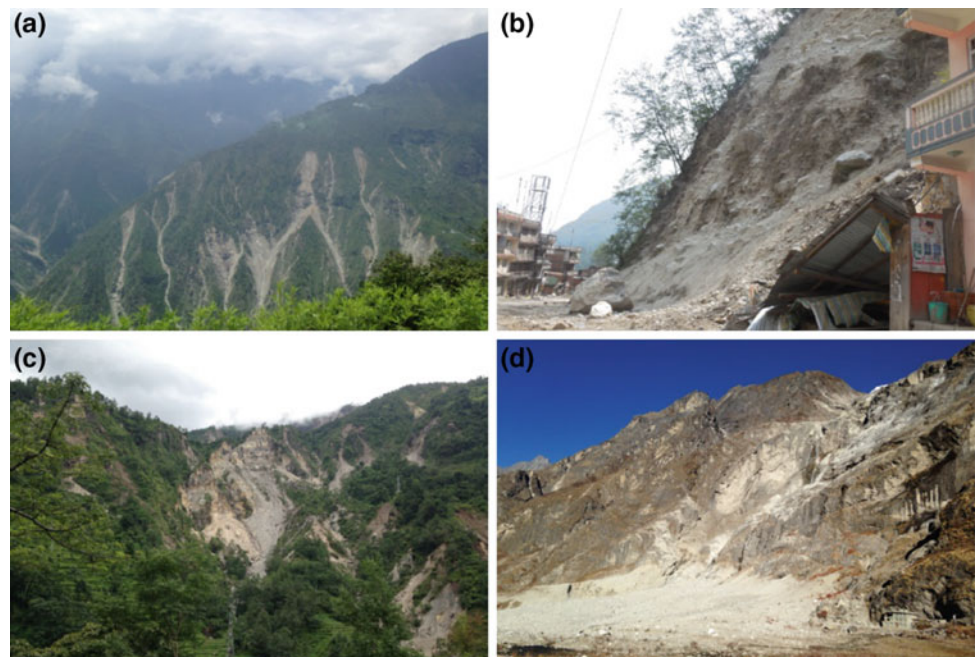


Fig. 2 Inventory of landslides triggered by the 2015 Gorkha earthquake on elevation model. The *red polygons* are landslides, *yellow star* is the mainshock epicentre $M_w = 7$ and the *dotted rectangle* is the

modelled seismogenic fault (USGS 2016). The cyan boundary is approximate boundary of landslide distribution and area of study (AoS)

Fig. 3 Photographs showing some landslide types triggered. **a** shallow seated disrupted slope failures; **b** individual rockfalls; **c** dry debris flow events; and **d** the disastrous large landslide in Langtang valley that buried a mountaineering trekking village



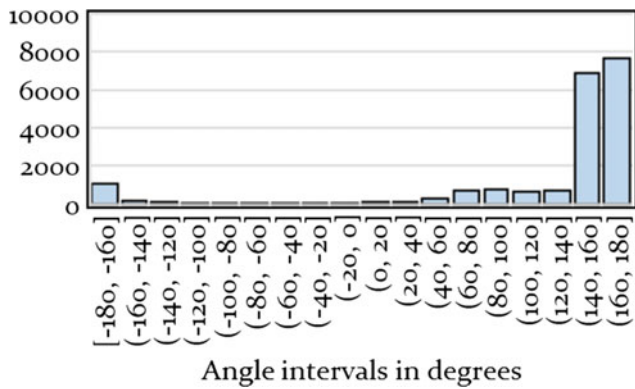


Fig. 4 Number of landslides versus epicentral angle

epi-center. Angle is counted from the east line reference to the epicenter in degrees, (refer Fig. 4).

Spatial Analysis of Landslides with Event Controlling Parameters

The event of an earthquake triggered landslide at a particular location is a function of various strong ground motion, geomorphic and geological characteristic parameters. Earthquake magnitude, fault geometry, distance from earthquake source and PGA comprise the strong ground motion parameters; slope angle, slope aspect and curvature

comprise the geomorphological parameters; and lithological composition comprise the geological parameter. The DEM was resampled to 5 m grid for analysis and 18,981 landslides with area greater than 30 m² were considered for further comparisons. This process although, does not improve the resolution further but it is done for consistency of landslides area considered and DEM pixel width. The following spatial correlation analysis was performed for the landslides, using two proxies of the co-seismic landslide abundance—(1) landslide area percentage (LAP) and (2) landslide top number percentage (LTP); compared to % of class area in the area of investigation.

Slope Angle

The slope map was derived from the Aster Global DEM (30 * 30 m) in ArcGIS. The slope range in the study area was 0°–89°, mean slope = 25.5° and standard deviation = 13. Landslides were observed in slope range 0°–80°, which was reclassified into 16 classes of 5° intervals including (1) 0°–5°, (2) 5°–10°, ..., (16) 75°–80°. Figure 5a shows the relation of landslides versus slope classes. The LAP and LNP values smoothly increase with increasing slope angle classes up to 40°–45° except angles greater than 45° because % slope class area also decreases beyond this range. Slopes higher than 30° appeared more susceptible to land sliding because beyond this range, most of rock types exceed their static

Fig. 5 a LAP and LNP versus classes of slope angle; b LAP and LNP versus classes of slope aspect

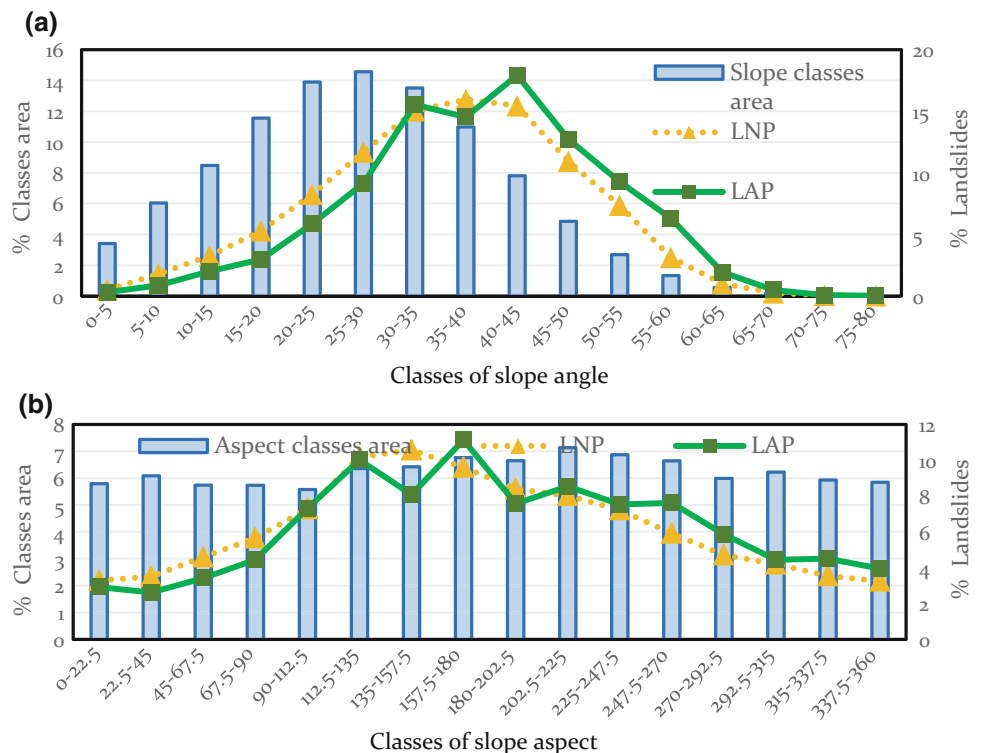
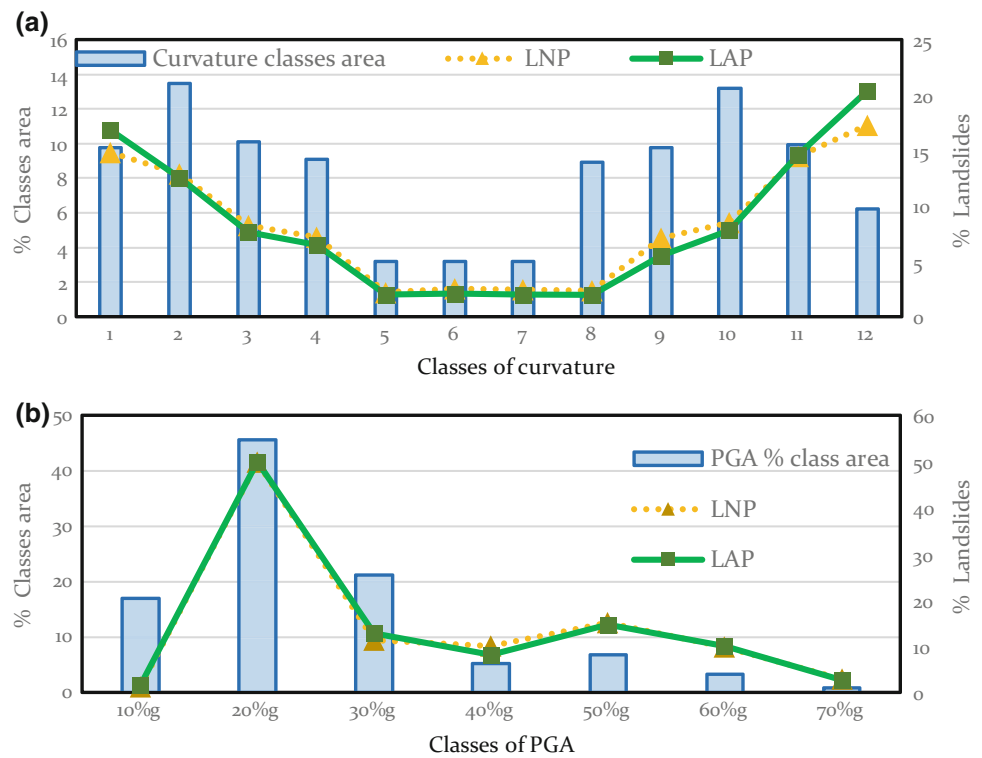


Fig. 6 **a** LAP and LNP versus classes curvature; **b** LAP and LNP versus classes of PGA



frictional strength and dynamic activation even disturbs their natural state of consolidation. As the slope angle increases, static shear stress develops in soil which cause the deformations to get accumulated downhill, leaving the upper portion loose and thus increases the transient strains and permanent slope displacements (Carlton et al. 2016). This increases the susceptibility of the landslide triggering crown areas in comparatively milder slope range.

Slope Aspect

Slope aspect is defined as the direction of maximum slope angle and is related to directional PGA (e.g. Dai et al. 2011), exposure to sunlight, drying winds, rainfall (degree of saturation) and discontinuities which may control landslide occurrence (Yalcin 2008). The aspect was classified into 16 classes of 22.5° intervals including (1) 0° – 22.5° , (2) 22.5° – 45° , ..., (16) 337.5° – 360° . Figure 5b shows the relation of landslides versus aspect classes. It can be found that class 5–11 (i.e. 112.5° – 247.5°); south-east-east to south-west-west facing slopes have relatively higher LND and LAD values than other directions which is consistent with rupture direction of the earthquake. Preferred directional acceleration (Carlton et al. 2016) could also have induced more susceptibility in these aspects and where much of the seismic energy release at the boundary interface in normal directions as landslides.

Curvature

Slope curvature could be a controlling factor for landslide occurrence as it could govern local topographic amplification effects. The slopes of negative curvature values represent concave surfaces, positive curvatures represent convex surfaces and a zero curvature means a flat surface. The curvature was classified into 12 classes including (1) <-2 , (2) -2 to -1 , (3) -1 to -0.5 , (4) -0.5 to -0.2 , (5) -0.2 to -0.1 , (6) -0.1 to 0 , (7) 0 to 0.1 , (8) 0.1 to 0.2 , (9) 0.2 to 0.5 , (10) 0.5 to 1 , (11) 1 to 2 and (12) $2>$. Correlation between this classification and LND- LAD are displayed in Fig. 6a. It is observed that increasing convexity and concavity induces larger landslides susceptibility and comparatively LNP and LAP values are slightly higher in the convex surfaces than the concave ones. There is diffraction and interference of seismic waves traveling in ridge-and- valley topography and this causes amplification of ground accelerations near ridge crests (Meunier et al. 2008). In our opinion, there was also a similar effect of local topographic amplification of seismic waves in ridges, spurs and valleys of the study area.

Peak Ground Acceleration

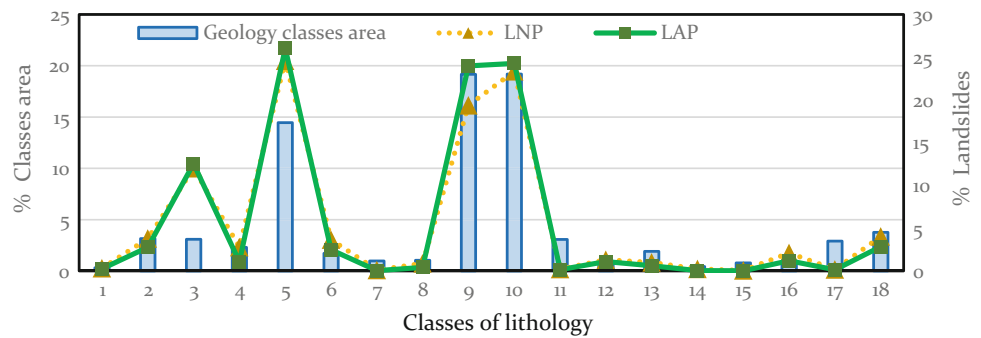
Modelled PGA map for the main shock event was accessed from USGS earthquake database and overlaid in the landslides distribution. Figure 6b shows the relationship between

Table 1 Geologic unit and description in the study area

Lithology (age)	Class	Formation	% Area	LAP	LNP
Basic rocks	1	Basic rocks	0.3	0.2	0.3
Shale, limestone, slate and sandstone (UPC-LP)	2	Galyang	3.2	2.8	3.8
Phyllite, slate, shale and limestone (UPC-LP)	3	Ghannapokhara	3.1	12.5	12.0
Gneiss (UPC-LP)	4	Gn	2.3	1.1	2.8
Gneiss, migmatite and marbles (PC-UPC)	5	Himal group	14.5	26.0	24.6
Limestone, dolomitic limestone and shale (UPC-LP)	6	Lakharpata	1.7	2.5	3.6
Sandstone, clay, siltstone, shale and conglomerate (MM-P)	7	Middle Siwalik	1	0.04	0.1
Quartzite and phyllite (UPC-LP)	8	Naudanda	1	0.4	0.9
–	9	No Data	19.2	24	19.4
Phyllite, quartzite, metasandstone and conglomerate (PC-UPC)	10	Ranimatta	19.2	24.3	23.3
Alluvium, boulder, gravel, sand and clay (MM-P)	11	Recent	3.1	0.1	0.2
Shales and dolomites (UPC-LP)	12	Sangram	1	1.1	1.3
Sandstone, gritstone, conglomerate and quartzite (UPC-LP)	13	Seti	2	0.6	1
Sandstone and mudstone (MM-P)	14	Chor Khola	0.4	0.03	0.2
Schist	15	Shiprin Khola	0.8	0.01	0.05
Quartzite, limestone, shales and sandstones (UPC-LP)	16	Syangja	1	1.2	2.1
Phyllite, slate, meta-sandstone, quartzite and limestone (UPC-LP)	17	Tistung	3	0.1	0.2
Schists, feldspar, quartz and gneisses (PC-UPC)	18	Ulleri	3.8	2.8	4.0

PC-UPC = Pre-Cambrian to Upper Pre-Cambrian, UPC-LP = Upper Pre-Cambrian to Late Paleozoic, MM-P = Middle Miocene-Pleistocene (data from DMG 2011)

Fig. 7 LAD and LND versus classes of lithological units



LNP, LAP and PGA classes of 0.1 g interval. It shows a strong correlation with increasing PGA values and there is a peak between 0.1 and 0.3 g at 0.2 g with all three parameters, i.e. % class area, LNP and LAP indicating the quasi static equilibrium condition of the predominantly young mountain formation with steeper topography and fragile geology which could be even triggered at very low PGA threshold value of 0.2 g. However, the largest recorded PGA (=0.241 g) was on the EW component at the rock site nearby

Kathmandu (Takai et al. 2016) which suggest less reliability of modeled values on the higher side.

Lithology

Geological formation map produced by the Department of Mines and Geology (National Database) in 1:250,000 scale was used to provide information of lithology in the study

area. Different lithological units have different susceptibility towards land sliding because of varying strength of rocks. Table 1 shows the various lithological units in 18 classes, time scale and corresponding LAP-LNP values which is also illustrated in Fig. 7. Low grade metamorphic rocks like gneiss, phyllite, slate, etc. dominant formation had high LAP and LNP values.

Conclusion

A total of 19,332 co-seismic landslides covering an area of 61.5 km² were mapped in 20,500 km² AoI triggered by the Gorkha earthquake using visual interpretation of satellite images in Google Earth. The various types of landslides include (1) shallow disrupted slope failures, (2) rock falls, (3) dry debris flows and (4) large landslides. Shallow disrupted slope failure was the major mode of landslide occurrence. The landslides distribution is primarily controlled by the rupture direction, seismo-genic fault and number density increases towards the SEE direction. The landslide concentration indices-LAP and LNP show a positive correlation with slope, aspect, curvature and PGA. Low-strength metamorphic rocks were most susceptible in terms of lithology. The landslide distribution and statistical results have a few differences to other earthquakes worldwide primarily with directional property and PGA threshold while the other values are unique to slope response to shallow- blind fault earthquakes in thrust fault Himalayan regions.

References

- Adhikari LB, Gautam UP, Koirala BP, Bhattarai M, Kandel T, Gupta RM, Hoste-Colomer R (2015) The aftershock sequence of the 2015 April 25 Gorkha—Nepal earthquake. *Geophys J Int* 203 (3):2119–2124
- Bettinelli P, Avouac JP, Flouzat M, Jouanne F, Bollinger L, Willis P, Chitrakar GR (2006) Plate motion of India and inter-seismic strain in the Nepal Himalaya from GPS and DORIS measurements. *J Geodesy* 80(8):567–589
- Bilham R, Larson K, Freymueller J (1997) GPS measurements of present-day convergence across the Nepal Himalaya, vol 386 (6620). Nature Publishing Group, pp 61–64
- Bollinger L, Henry P, Avouac JP (2006) Mountain building in the Nepal Himalaya: thermal and kinematic model. *Earth Planet Sci Lett* 244(1):58–71
- Carlton B, Kaynia AM, Nadim F (2016) Some important considerations in analysis of earthquake-induced landslides. *Geoenviron Disasters* 3(11):1–9
- Collins BD, Jibson RW (2015) Assessment of existing and potential landslide hazards resulting from the April 25, 2015 Gorkha, Nepal earthquake sequence (No. 2015–1142). US Geological Survey
- Cui P, Chen XQ, Zhu YY, Su FH, Wei FQ, Han YS, Zhuang JQ (2011) The Wenchuan earthquake (May 12, 2008), Sichuan province, China, and resulting geohazards. *Nat Hazards* 56(1):19–36
- Dai FC, Xu C, Yao X, Xu L, Tu XB, Gong QM (2011) Spatial distribution of landslides triggered by the 2008 Ms 8.0 Wenchuan earthquake, China. *J Asian Earth Sci* 40(4):883–895
- Dimri S, Lakhara RC, Sati S (2007) Fuzzy-based method for landslide hazard assessment in active seismic zone of Himalaya. *Landslides* 4 (2):101–111
- DMG (2011). Geological map of Eastern Nepal (1:250000). Department of Mines and Geology (DMG). Geological mapping section.
- Elliott JR, Jolivet R, González PJ, Avouac JP, Hollingsworth J, Searle MP, Stevens VL (2016) Himalayan megathrust geometry and relation to topography revealed by the Gorkha earthquake. *Nat Geosci* 9:174–180
- Government of Nepal (2016) Nepal Earthquake 2015: Country profile. ICMOD Geoportal. <http://apps.geoportal.icimod.org/NDRRIP/profile?id=Country&Lang=en>. Accessed 28 Jun 2016
- Grandin, R., Vallée, M., Satriano, C., Lacassin, R., Klinger, Y., Simoes, M., Bollinger, L. (2015). Rupture process of the Mw = 7.9 (2015) Gorkha earthquake (Nepal): insights into Himalayan megathrust segmentation. *Geophys Res Lett* 42(20):8373–8382
- Hashash YM, Tiwari B, Moss RE, Asimaki D, Clahan KB, Kieffer DS, Pehlivan M (2015) Geotechnical field reconnaissance: Gorkha (Nepal) earthquake of April 25, 2015 and related shaking sequence. Geotechnical Extreme Event Reconnaissance GEER Association Report No. GEER-040, pp 1–250
- Kargel JS, Leonard GJ, Shugar DH, Haritashya UK, Bevington A, Fielding EJ, Anderson E (2016) Geomorphic and geologic controls of geohazards induced by Nepal's 2015 Gorkha earthquake. *Science* 351(6269):aac8353
- Keefer DK (1984) Landslides caused by earthquakes. *Geol Soc Am Bull* 95(4):406–421
- Keefer DK (2000) Statistical analysis of an earthquake-induced landslide distribution — the 1989 Loma Prieta. *California event Eng Geol* 58(3–4):231–249
- Keefer DK (2002) Investigating landslide caused by earthquakes—a historical review. *Surv Geophys* 23(6):473–510
- Meunier P, Hovius N, Haines JA (2008) Topographic site effects and the location of earthquake induced landslides. *Earth Planet Sci Lett* 275:221–232
- Qi S, Xu Q, Lan H, Zhang B, Liu J (2010) Spatial distribution analysis of landslides triggered by 2008.5.12 Wenchuan Earthquake, China. *Eng Geol* 116(1–2):95–108
- Rodriguez CE, Bommer JJ, Chandler RJ (1999) Earthquake-induced landslides: 1980–1997. *Soil Dyn Earthq Eng* 18(5):325–346
- Takai N, Shigefuji M, Rajaure S, Bijukchhen S, Ichiyani M, Dhital MR, Sasatani T (2016) Strong ground motion in the Kathmandu Valley during the 2015 Gorkha, Nepal, earthquake. *Earth Planets Space* 68(1):1
- USGS (2016) Earthquake Hazards Program. <http://earthquake.usgs.gov/earthquakes/eventpage/us20002926#shakemap>. Accessed 10 July 2016
- Wang HB, Sassa K, Xu WY (2007) Analysis of a spatial distribution of landslides triggered by the 2004 Chuetsu earthquakes of Niigata prefecture. *Japan Nat Hazards* 41(1):43–60
- Xu C (2014) Preparation of earthquake-triggered landslide inventory maps using remote sensing and GIS technologies: principles and case studies. *Geosci Front* 6(6):825–836
- Xu C, Xu X, Dai F, Xiao J, Tan X, Yuan R (2012) Landslide hazard mapping using GIS and weight of evidence model in Qingshui river watershed of 2008 Wenchuan earthquake struck region. *J Earth Sci* 23:97–120
- Xu C, Xu X, Yao X, Dai F (2014a) Three (nearly) complete inventories of landslides triggered by the May 12, 2008 Wenchuan Mw 7.9 earthquake of China and their spatial distribution statistical analysis. *Landslides* 11(3):441–461

- Xu C, Shyu JBH, Xu X (2014b) Landslides triggered by the 12 January 2010 Port-au-Prince, Haiti, M-w = 7.0 earthquake: visual interpretation, inventory compiling, and spatial distribution statistical analysis. *Nat. Hazards Earth Sys Sci* 14(7):1789–1818
- Yalcin A (2008) GIS-based landslide susceptibility mapping using analytical hierarchy process and bivariate statistics in Ardesen (Turkey): comparisons of results and confirmations. *CATENA* 72 (1):1–12